SUPPLEMENTARY MATERIAL FOR:

Klesner, C., R. Crawford, J. Vieri & M. Martinón-Torres. 2026. **A method to assess inter- and intra-vessel shape variation in pottery using outline-based geometric morphometrics.** *Antiquity*

S0. Resumen

Un método para evaluar varaciones morfológicas intra y entre recipientes cerámicos empleando morfometría geométrica

Las variaciones en la forma cerámica pueden aportar información clave sobre aspectos de la organización artesanal, como la estandarización y la destreza de los alfareros. Aunque algunos estudios han empezado a desarrollar métodos cuantitativos para comparar formas, apenas se ha explorado la posibilidad de documentar e interpretar variaciones internas en la forma de un recipiente cerámico.

Este estudio introduce un método cuantitativo para evaluar la variación morfológica de los recipientes a partir de mediciones métricas y morfometría geométrica (GMM), aplicadas a modelos 3D empleando software de código abierto. Estas medidas se utilizan para comparar formas entre conjuntos cerámicos distintos, pero también variaciones internas en la forma de cada recipiente. Se evaluaron mediciones métricas como redondez, circularidad y variaciones en el grosor de las paredes, así como la novedosa métrica de distancia al centroide del grupo (D_{Group}), calculada a partir de múltiples secciones virtuales de cada vasija analizadas mediante GMM basada en contornos. Consideradas en conjunto, estas métricas tienen el potencial de revelar hábitos motores idiosincrásicos de alfareros individuales, dentro de comunidades de práctica.

Presentamos un estudio de caso de 30 cuencos con pedestal ("copas") procedentes de la Serranía nariñense (Colombia), que representan las tradiciones cerámicas Capulí, Piartal y Tuza, para demostrar la aplicación del método. Los resultados revelan patrones diferenciados de variabilidad morfológica entre las tradiciones: las vasijas Capulí muestran los niveles más altos de variación inter- e intrarecipiente, lo que sugiere una producción descentralizada, con artesanos de diferentes grados dehabilidad. Por su parte, las vasijas Piartal y Tuza presentan una variabilidad general menor y mayor simetría rotacional, consistentes con manufactura más hábil o estandarizada. Aunque existe variación dentro de cada tradición, y teniendo en cuenta el tamaño reducido de la muestra, no se identifican diferencias marcadas en la estandarización interna ni en la simetría rotacional entre Piartal y Tuza. Este hallazgo resulta significativo, ya que se ha argumentado recientemente que las vasijas Tuza reflejan la introducción de ideas o conocimientos técnicos foráneos, evidentes en nuevas técnicas decorativas (Klesner *et al*. 2025). Más allá de un ligero incremento en la circularidad, la adopción de este nuevo conocimiento técnico no parece haber estado acompañada de un aumento en la estandarización del producto.

Una línea de investigación especialmente prometedora es el estudio de la variabilidad dentro de depósitos individuales, como las tumbas, donde la variación morfométrica del conjunto podría reflejar diferentes hábitos motores y, en consecuencia, la participación de distintos productores. Como ejemplo, las vasijas de un único contexto funerario Piartal en el sitio CIAO21 (Obonuco) mostraron amplios rangos de variabilidad en las métricas analizadas, lo que indica que los objetos depositados en esta tumba fueron probablemente elaborados por múltiples individuos con niveles de destreza distintos.

Este estudio subraya el valor de integrar parámetros métricos y morfológicos extraídos de modelos 3D para analizar tradiciones cerámicas, y comparte métodos de código abierto para facilitar su aplicación en otros estudios. El enfoque propuesto para evaluar la variación morfológica de los recipientes resulta

aplicable a un amplio espectro de conjuntos y formas cerámicas, y ofrece una visión más matizada de las prácticas tecnológicas del pasado.

S1. Archaeological Context

The sample of thirty ceramic vessels consist of artefacts from recently excavated sites in Nariño, Colombia as well as from archaeological pottery collections. The context of each has been described in Klesner *et al*. (2025) and summarised here.

The excavated material includes samples from **Site 137** in El Porvenir, Iles (Mendoza Acosta & Rubin de Rubin 2021; Mendoza Acosta & Marín 2023) which was excavated in 2019-2020 as part of the preventive archaeological interventions carried out within the Rumichaca-Pasto Road Project (ICAHN registration no. 7610). The site, which is dated to the 4-5th c. AD, is a cemetery, and only Capulí style ceramics were recovered from the tombs. There was no evidence of looting or high agricultural activity at the site, which resulted in undisturbed tombs with remarkably well-preserved ceramic vessels.

Two different excavations in the municipality of Catambuco are considered in this research. Catambuco is located approximately 4 km south of the major city of Pasto, and the sites are located above 2800 m.a.s.l. **Site 8** was excavated as part of the preventive archaeology study (ICAHN registration no. 4627) of the Rumichaca-Pasto Road Project, and recovered only Piartal style ceramics from a total of eight excavated tombs, three of which were undisturbed.

Adjacent and immediately below Site 8 is the site of **San Damián**, which was excavated as part of a preventive archaeology study (ICANH permit No. 7774 and 8066) for the CESMAG University Institution project. The study area is a large plateau (78,434 m^2), which includes domestic, funerary, and ceremonial contexts. Archaeological evidence suggests that the site was primarily associated with Tuza ceramic material, and is related to a late pre-Hispanic occupation.

Lastly the site of **CIAO21** is located on the land of the AGROSAVIA research centre in Obonuco, Pasto excavated in 2021 as part of the "ICAHN Protocol for the Management of Chance Archaeological Finds". The site consists of just one, exceptional communal tomb that dates from the 11th-12th c. AD (Maya Cabrera 2024). The tomb consisted of fourteen individuals (nine adults and five infants), 59 complete or near complete Piartal style ceramic vessels, along with lithic artifacts, an ocarina, textile fragments, necklace beads, and a sample of ochre pigment.

The excavated material was supplemented with material in the **Museo del Oro** in Bogotá, which has a large corpus of ceramic from the Narino highlands. A second pottery collection, the Hacienda San Antonio de Bomboná Pottery collection (abbreviated to **Bomboná collection**), which is registered with the Colombian Institute of Anthropology and History (ICANH) under the 'Resolución de tenencia de patrimonio arqueológico colombiano' (ICANH registration no. 1202), was also examined.

Vessel morphology

30 vessels broadly defined as a bowl with a pedestal foot, also referred to as *copa*, *compotera*, *cuenco con soporte,* and *cuenco con base anular*, were analysed in this study. This shape was chosen for morphological analysis for several reasons: 1) the general shape is present in all three wares, 2) it is the most common vessel shape included in burial contexts, and 3) as an open vessel, we can gain insights into the morphology and other technological aspects such as wall thickness, which are not available in closed vessel forms documented by structured light 3D scanning. The prior morphological study included outline-based GMM analysis of cross-sections of 85 vessels and confirmed the distinction between Capulí, Piartal, and Tuza wares, as well as determining the level of morphological standardisation within each of these.

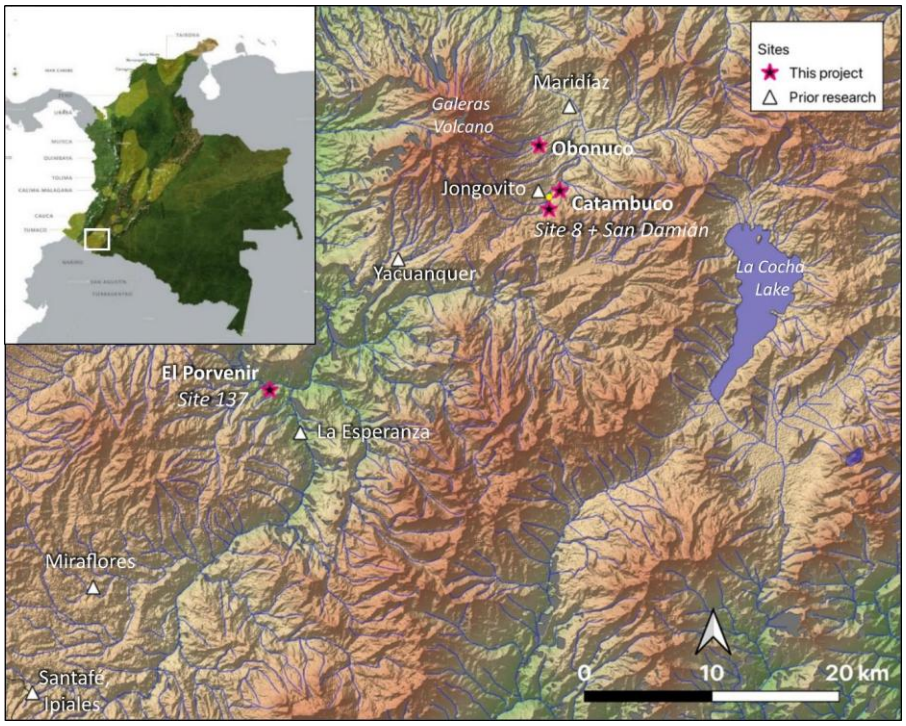

Figure S1. Map of the Serranía nariñense (Colombia) with the location of the sites mentioned in the text indicated. Map drawn in QGIS v. 3.4.4 (QGIS Development Team 2022) with the projection Magna-Sirgas EPSG 4686. Hillshade based on 1 Arc-Second STRM data produced by NASA, with the water bodies taken from Instituto Geográfico Agustín Codazzi (IGAC 2022).

Table S1. Summary of the samples included in this analysis, including their archaeological context where known.

Vessel	Ware	Collection	Context
CA230334	Capulí	Museo del Oro	None
CA230335	Tuza	Museo del Oro	None
CA230337	Piartal - 2	Museo del Oro	None
CA230347	Piartal - 2	Museo del Oro	None
CA230348	Capulí	Museo del Oro	None
CA230354	Tuza	Museo del Oro	None
CA230361	Piartal - 1	Catambuco - Site 8	Monitoreo, Tomb 3
CA230365	Capulí	El Porvenir - Site 137	Corte 7, Tomb 1
CA230366	Capulí	El Porvenir - Site 137	Corte 7, Tomb 1
CA230375	Capulí	El Porvenir - Site 137	Monitoreo, Tomb 2
CA230377	Capulí	El Porvenir - Site 137	Landslide, Tomb 4
CA230378	Capulí	El Porvenir - Site 137	Landslide, Tomb 4
CA230381	Capulí	El Porvenir - Site 137	Landslide, Tomb 10
CA230386	Capulí	El Porvenir - Site 137	Landslide, Tomb 1
CA230387	Capulí	El Porvenir - Site 137	Landslide, Tomb 5
CA230401	Tuza	Bomboná	Attributed to the Los Eucaliptos homestead
CA230404	Piartal - 2	Bomboná	Attributed to Aguacate homestead
CA230411	Tuza	Bomboná	Attributed to Aguacate homestead
CA230416	Piartal - 1	CIAO21	Obonuco tomb
CA230417	Piartal - 1	CIAO21	Obonuco tomb
CA230422	Piartal - 1	CIAO21	Obonuco tomb
CA230423	Piartal - 1	CIAO21	Obonuco tomb
CA230424	Piartal - 1	CIAO21	Obonuco tomb
CA230428	Tuza	Catambuco - San Damián	Rasgo 36, Tomb 18
CA230429	Tuza	Catambuco - San Damián	Rasgo 95, Tomb 50
CA230430	Tuza - Red slip	Catambuco - San Damián	Monitoreo
CA230715	Tuza	Museo del Oro	None
CA230717	Piartal - 1	Museo del Oro	None
CA230718	Tuza	Museo del Oro	None
CA230724	Tuza	Museo del Oro	None

S2. Processing of Cross-sections and Selection of Harmonics for EFA

Calculation of Cross-section completeness

When considering intravessel variation, we were cognisant that our approach could introduce more variation in vessels that had higher degrees of alteration resulting from their use or deposition. We did not want to capture variation that resulted in cracks, breakage, or pitting resulting from ware, but variation that was the result of the original shaping of the vessel. Vessels from Site 137 (Klesner *et al*. 2025), including those beyond the scope of this study, were assessed as they had a range of preservation conditions, from minimal (CA230366) to high (CA230384) degrees of post-production alteration. We conducted the GMM analysis considering different thresholds of completeness (see Table S2).

Images were first processed using image-editing software (Inkscape) to digitally infill missing components of the vessel cross-sections with red, following standard archaeological illustration practices. We then applied an automated R script that read each image, identified red, black, and white pixels based on RGB thresholds, and calculated the proportion of red pixels relative to red + black pixels for each vessel section.

Table S2. Results showing the average distance to the centroid (D_{Group}) and number of cross-sections retained for each vessel when considering different completeness thresholds.

Vessel	Only complete		>99% preserved		>95% preserved		>90% preserved		all cross-sections	
	N=	D_{Group}	N=	D_{Group}	N=	D_{Group}	N=	D_{Group}	N=	D_{Group}
CA230355	19	0.09099	25	0.11000	26	0.11782	28	0.15917	36	0.29931
CA230358	-	-	-	-	-	-	7	0.09719	36	0.35634
CA230359	21	0.05958	21	0.05958	30	0.14240	36	0.15148	36	0.15148
CA230365	23	0.12466	34	0.11415	36	0.11477	36	0.11477	36	0.11477
CA230366	32	0.04164	32	0.04164	36	0.04139	36	0.04139	36	0.04139
CA230372	14	0.02392	19	0.02992	30	0.11962	36	0.16462	36	0.16462
CA230373	18	0.01540	26	0.02136	36	0.03458	36	0.03458	36	0.03458
CA230374	19	0.04654	29	0.05564	36	0.05989	36	0.05989	36	0.05989
CA230376	23	0.01391	25	0.01732	31	0.04884	36	0.09122	36	0.09122
CA230377	30	0.04337	36	0.04606	36	0.04606	36	0.04606	36	0.04606
CA230378	17	0.04243	34	0.05066	36	0.05531	36	0.05531	36	0.05531
CA230380	31	0.21640	35	0.21905	36	0.23803	36	0.23803	36	0.23803
CA230381	26	0.01503	36	0.01996	36	0.01996	36	0.01996	36	0.01996
CA230382	18	0.03094	28	0.03888	36	0.04295	36	0.04295	36	0.04295
CA230384	-	-	-	-	-	-	14	0.15725	36	0.15537
CA230386	29	0.05149	31	0.05603	36	0.06394	36	0.06394	36	0.06394
CA230387	28	0.03666	33	0.03701	36	0.03878	36	0.03878	36	0.03878
CA230388	11	0.03893	11	0.03893	13	0.05802	17	0.16451	36	0.30571

Completeness thresholds were evaluated by calculating the change in D_{Group} (Δ) for each vessel relative to its 100% completeness baseline (Figure S2). While both >99% and >95% completeness thresholds yielded low mean Δ values (0.004 and 0.022, respectively), the shift from >99% to >95% represented a fivefold increase in measured average variation, with some vessels notably increasing their variation likely reflecting minor post-depositional alterations rather than original vessel form. To limit the introduction of this post-depositional alteration while still retaining some incomplete sections for analysis to increase the number of objects which can be assessed by this method, we adopted the >99% completeness threshold for subsequent GMM analyses.

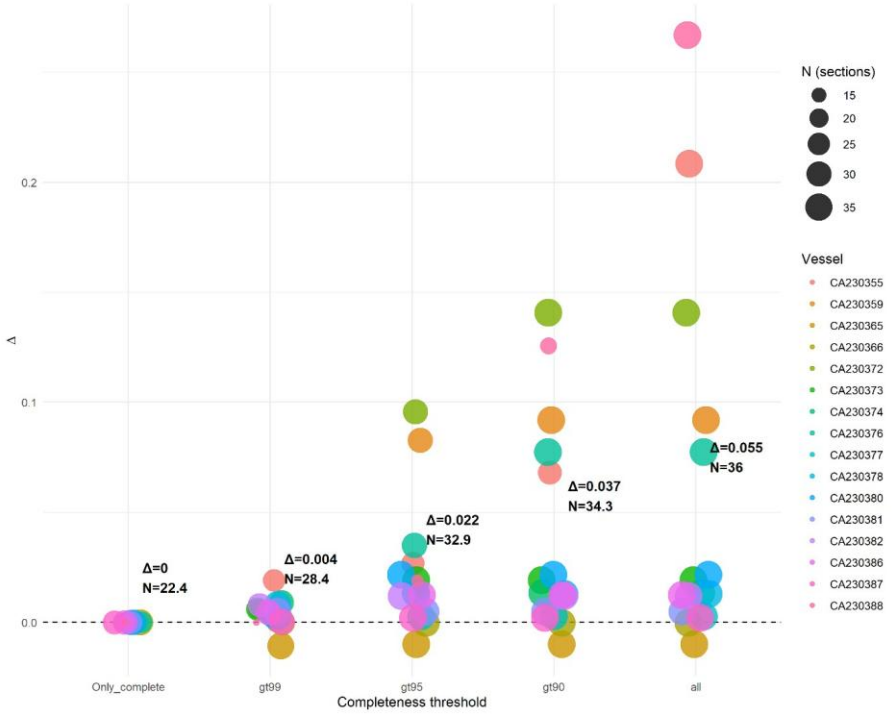

Figure S2. Change in D_{Group} (Δ) for each vessel relative to its 100% completeness baseline across decreasing completeness thresholds (>99%, >95%, >90%, and all cross-sections). Δ values were calculated as the difference between the D_{Group} at a given threshold and the D_{Group} at 100% completeness for the same vessel. Each point represents a vessel at a given threshold, with colours distinguishing vessels and point size proportional to the number of cross-sections (N) contributing to that threshold. Mean Δ and mean N across vessels are reported.

Considering Harmonics

Outline-based geometric morphometrics (GMM) characterises an object's 2D outline as a closed polygon (Bonhomme *et al.* 2014) which can then be expressed numerically through Elliptic Fourier Analysis (EFA), which encodes the contour of the polygon as trigonometric series whose harmonic coefficients describe the shape (Kuhl & Giardina 1982; Bonhomme *et al.* 2014; Cortell-Nicolau *et al.* 2023). The number of harmonics determines the quality and precision of the geometric representation of the object (Wang & Marwick 2020). Lower harmonics provide approximations for the coarse-scale trends, while higher frequency harmonics can be used to identify fine-scale variations (Bonhomme *et al*. 2014). The selection of the number of harmonics is thus an important consideration in EFA, and must be assessed in every study and considered through exploratory analyses (Ioviţă 2009). Harmonic power, which is computed as a cumulative sum of squared harmonic coefficients, provides a practical rule for choosing how many harmonics to retain to avoid under or over-sampling, with 99% often set as the threshold for outline-based GMM studies (Bonhomme *et al.* 2014; Wang & Marwick 2020; Loftus 2022). However, adding harmonics beyond this power threshold will inform about more minute

variations in object morphology, like those of interest for intra-vessel variation. At the same time, it is important not to overfit the data by selecting too many harmonics which would pick up "noise" resulting from artefacts in the sample collection or defects not of interest in the objects themselves.

For this study, we retained 30 harmonics for the EFA, although 8 harmonics captured 99% and 17 harmonics captured 99.9% of the total harmonic power in the elliptic Fourier coefficients. Overall, 30 harmonics yielded the same overall interpretation as those calculated using 17 harmonics (see Figures S4 and S5, Table S3), however the higher cut-off better resolved the subtle morphological differences highlighted by our PCA. Along PC2 (Fig. S5), shapes shift from a flat underside of the base at negative scores to a gently undulating underside at positive scores, characterised by two shallow concave depressions near the base–wall junction flanking a slight central convexity (a low boss). These local curvature features are only resolved when using 30 harmonics; with fewer harmonics they are smoothed out. On this basis, 30 harmonics provided a prudent balance between capturing fine-scale morphology and avoiding noise, while leaving the substantive conclusions unchanged.

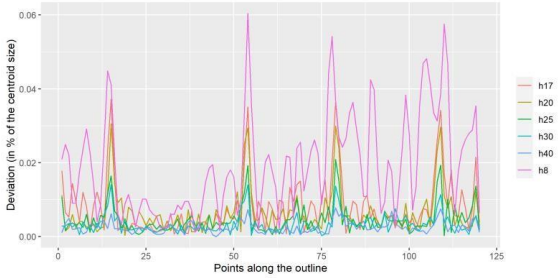

Figure S3. Plot showing the deviation in total percentage of the centroid size between the best possible fit with a given number of harmonics (8, 17, 20, 25, 30, and 40) for sampled points along the outline (on the x-axis).

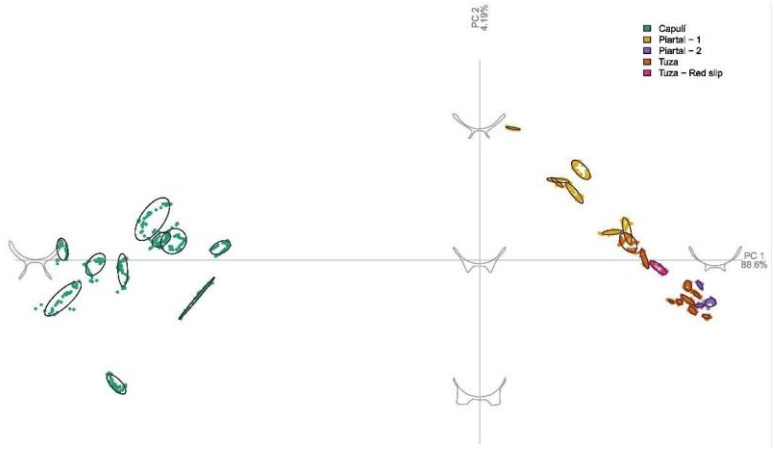

Figure S4. Biplot of PC1 vs PC2 for all cross-sections >99% preserved, using only 17 harmonics for EFA, with the ware of the sections indicated in colour, and ellipses overlaid indicating 90% confidence intervals for cross-sections from individual vessels.

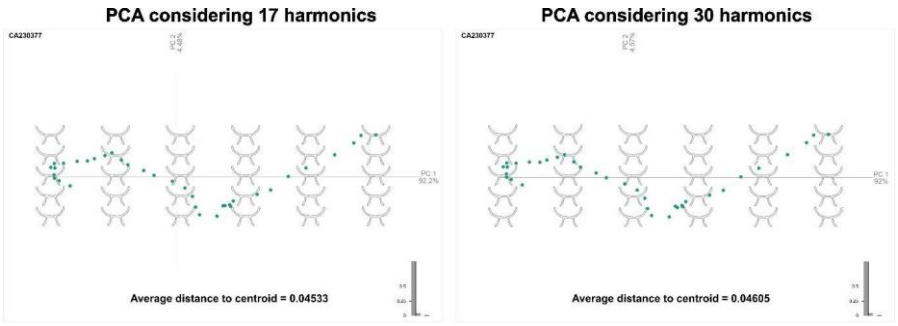

Figure S5. PC1 versus PC2 for the 36 cross-sections for CA230377, considering (*left*) 17 harmonics and (*right*) 30 harmonics.

Table S3. Results showing the average distance to the centroid (D_{Group}) for each vessel and ware considering 17 and 30 harmonics, and the relative percentage difference between the two.

Vessel	Ware	D_{Group} – 30 harmonics		D_{Group} – 17 harmonics		Relative Percentage Difference
		Vessel	Ware	Vessel	Ware	
CA230334	Capulí	0.08898		0.08790		1%
CA230348	Capulí	0.03919		0.03847		2%
CA230365	Capulí	0.11413		0.11258		1%
CA230366	Capulí	0.04164	0.05361 ±	0.04096	0.05283 ±	2%
CA230375	Capulí	0.04220	0.0276	0.04165	0.02728	1%
CA230377	Capulí	0.04605		0.04533		2%
CA230378	Capulí	0.05063	CV = 52%	0.04987	CV = 52%	2%
CA230381	Capulí	0.01993		0.01957		2%
CA230386	Capulí	0.05602		0.05495		2%
CA230387	Capulí	0.03736		0.03700		1%
CA230361	Piartal - 1	0.02793		0.02748		2%
CA230416	Piartal - 1	0.03965		0.03887		2%
CA230417	Piartal - 1	0.02599		0.02554		2%
CA230422	Piartal - 1	0.01268	0.02428 ±	0.01250	0.02379 ±	1%
CA230423	Piartal - 1	0.01666	0.0090	0.01633	0.00877	2%
CA230424	Piartal - 1	0.03677		0.03609		2%
CA230717	Piartal - 1	0.01795	CV = 37%	0.01764	CV = 37%	2%
CA230347	Piartal - 2	0.02321		0.02256		3%
CA230404	Piartal - 2	0.02635		0.02556		3%
CA230337	Piartal - 2	0.01563		0.01533		2%
CA230335	Tuza	0.01247		0.01217		2%
CA230354	Tuza	0.02737		0.02677		2%
CA230401	Tuza	0.01891		0.01863		2%
CA230411	Tuza	0.02662	0.02207 ±	0.02611	0.02159 ±	2%
CA230428	Tuza	0.01324	0.0074	0.01293	0.00729	2%
CA230429	Tuza	0.01808		0.01765		2%
CA230715	Tuza	0.02403	CV = 34%	0.02328	CV = 34%	3%
CA230718	Tuza	0.02668		0.02590		3%
CA230724	Tuza	0.03626		0.03570		2%
CA230430	Tuza – Red slip	0.01705		0.01677		2%

Commented [CK1]: Please make sure that the table is all on one page

S3. Wall-thickness as a proxy for primary forming method

Two recent publications have presented methods to quantify intra-vessel variation in wall thickness and shape regularity (Thér & Wilczek 2022; Caloi & Bernardini 2024). Both studies have examined open vessel shapes made experimentally by a single, skilled potter employing a range of forming methods (Table S4).

Table S4. Summary of the forming methods, analytical techniques, and measures of variability examined in recent experimental archaeology studies.

Study	Forming methods under investigation	Sample size	Analytical Method	Measure of Variability
Caloi & Bernardini 2024	Throwing-off-thehump Wheel-throwing from a solid ball of clay Wheel-pinching Wheel-coiling	60 vessels were made, but only 12 vessels, three made by each forming method, were analysed	Micro-CT scanning	**Vertical Wall thickness**
				3D visualisation of wall thickness
				3D visualisation of void orientation
Thér & Wilczek 2022	Coiling with turntable finishing (CTF) Coiling with potter's wheel finishing (CWF) Wheel-thrown (WT)	27 vessels, nine made by each forming method, considering three sections from each	Artec Space Spider 3D structured light scanner	**Horizontal Wall thickness** Mean Range standard deviation
				Surface regularity mean height (Ra) maximum height (Rz) root mean square height (Rq)

Thér and Wilczek examined ceramics that were made by three different methods employing different degrees of rotational energy: 1) coiling combined with wheel finishing using a turntable, 2) coiling combined with wheel finishing on a potter's wheel, and 3) wheel throwing. They examined nine vessels made by each technique. The raw data from the Thér and Wilczek study was made available to us for comparison with our archaeological samples. While Thér and Wilczek considered the consistency in wall thickness at multiple different areas of the vessel (the neck, maximum body diameter, and lower portion of the body), in our comparison, we only considered the maximum body diameter, as it was the most analogous point to where we selected the horizontal section in our study. We analysed the wall thicknesses of their vessels following the same protocol as our archaeological ceramics, and randomly selected nine of the coil-made ceramics in our study for comparison.

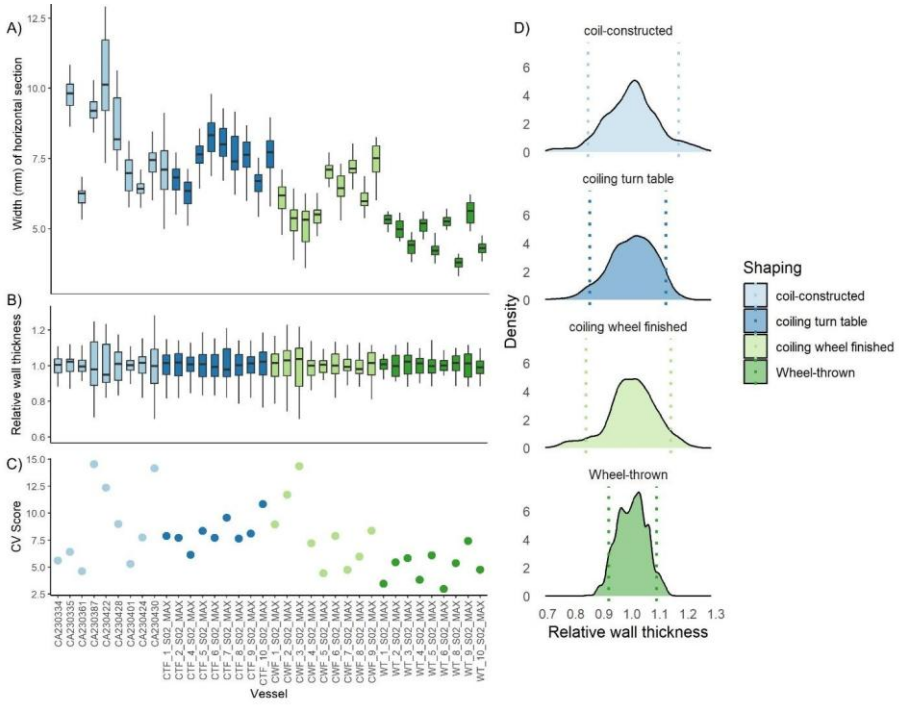

Figure S6. The distribution of vessel wall thickness values calculated from horizontal sections of individual vessels made by different forming methods, grouped by those forming methods. Coil-constructed data from this study, all others from Thér & Wilczek (2022). A) The distribution of 200 width values taken sequentially for each vessel. B) The values of the widths divided by the mean widths for the vessel. C) The CV calculated from the 200 measurements for each vessel. D) Density plots for all vessels grouped by their forming methods, with the 90% range marked by the vertical dashed lines.

We observe similar intra-vessel variation on the samples that were made by coiling, coiling with turntable finishing, and coiling with potter's wheel finishing (Figure S6). Only the wheelthrown vessels had significantly lower levels of variation in the thickness of their walls. Caloi & Bernardini (2024) also observed a difference in wall-thickness variation between those made by rotative kinetic energy (Throwing-off-the-hump and Wheel-throwing from a solid ball of clay) and hand-building methods aided by a wheel (Wheel-pinching and Wheel-coiling) when examining the variation through 3D visualisation of wall thickness and 2D vertical cross-sections of the vessels. Those made by RKE had relatively standardised wall thickness while those that were hand-built had more irregular wall thickness. These results suggests that variability in wall-thickness variation arises from the primary method of forming. Wall-thickness variation, especially as captured by horizontal sections (Figure S6), is a promising metric to identify the technological process of forming in archaeological assemblages, used in tandem with other metric measurements.

S3. Calculating CVs on dimensionless data

Previous studies attempting to quantify variability in morphology from outline-based GMM data have calculated the CV from normalised PC scores (Wang & Marwick 2020; Loftus 2022; Smallwood *et al.*

2022). The need for normalised PC scores is described in Wang and Marwick (2020: 5) as necessary 'given that CVs are most informative when computed on either all positive values or all negative values.' They therefore normalised the values to range from 1 to 10. However, when normalising inherently dimensionless PC scores to all positive values, samples which have PC scores that were originally positive are shifted to be more positive and will have a higher normalised mean resulting in a lower CV score, while values that were initially negative will have a lower average mean, and thus a higher CV score and will be interpreted as having less standardisation. This can be demonstrated when examining data produced by Wang and Marwick (2020), which we were able to re-analyse because of their good practice in making it fully available on github. We use it to demonstrate problems with the method, not the data.

Following outline-based GMM, they observed modest morphological distinction between vessels made during the Pre-European, Post-European, and Chinese phases (Figure S7). Vessels from the Chinese phase had positive PC1 scores and mostly negative PC2 scores, while vessels assigned as Pre- and Post-European phases ranged across both axes. In their assessment of the CV scores calculated from the normalised PC's, they found significant differences in pottery shape and shape standardisation that indicated changes in pottery production resulting from contact with mainland Han Chinese groups in north-eastern Taiwan. They identified that the lower CV score in PC1 seen in the Chinese vessels (15%) compared to the higher variation in the earlier pre-European (33%) and post-European (31%) period vessels as indicating a trend towards standardisation in shape over time.

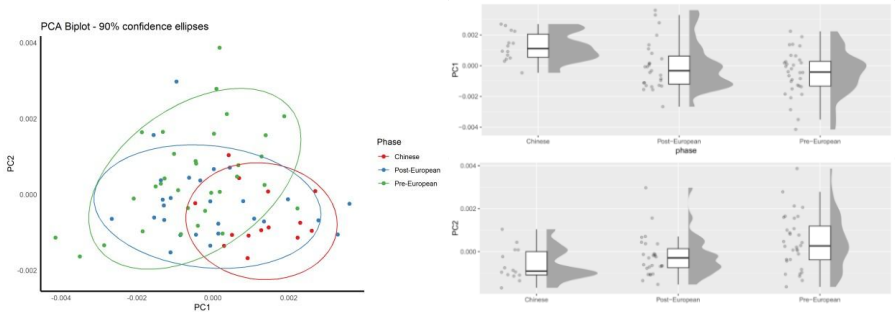

Figure S7. (*Left*) Biplot of PC1 vs PC2 for samples from Wang and Marwick (2020) distinguished by phase with 90% confidence ellipses overlaid, and (*Right*) distribution of PC scores by phase.

However, if their original PC plots were inversed (Supplementary Figure 8), which would not change the interpretation of their morphology as PC scores are inherently dimensionless, the difference in CV would be much less pronounced (29% in the Chinese vessels versus 30% and 35% in the Pre- and PostEuropean period, respectively). They also considered standard, metric measurements when considering standardisation, and saw a much more modest difference in variation in body diameter between then Chinese (CV=8%) compared to the Pre- (CV=11%) and Post-European (CV=12%) vessels.

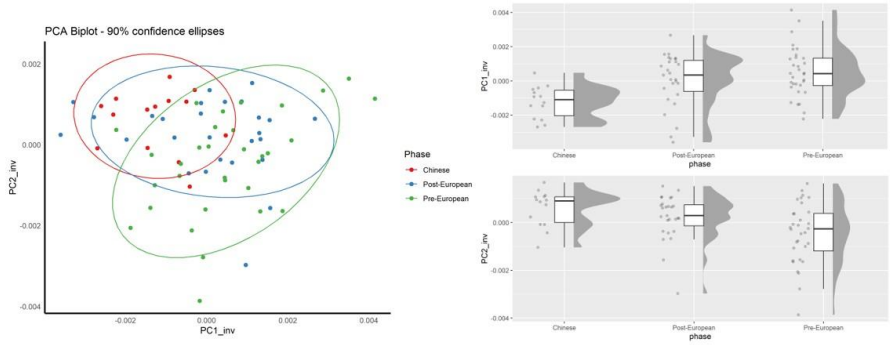

Figure S8. (*Left*) Inversed biplot of PC1 vs PC2 for samples from Wang and Marwick (2020) distinguished by phase with 90% confidence ellipses overlaid, and (*Right*) inversed distribution of PC scores by phase.

We calculated the group distance to the centroid value (D_{Group}) for the samples in Wang and Marwick's study and conducted a permutation test of homogeneity of multivariate dispersion (PERMDISP). This test consists of measuring the distance between all individual group members (vessels) and the group (phase) centroid in multivariate principal coordinates analysis (PCoA) space using the betadisper function of the vegan package in R (Oksanen *et al.* 2024). Groups (phase) with more variance will have larger mean distance to the centroid values (Table S5). While the results suggest that the Chinese vessels showed modestly lower levels of variation having a lower D_{Group} value compared to the Pre- and Post-European phases, the results of the ANOVA showed that the differences in the dispersion of the vessels were not significant (F=1.3398, p = 0.2685).

Table S5. The average distance to the centroid for each phase considering 48 PCs.

Phase	**Sample size**	**D_{Group}**
Chinese	14	.0159
Post-European	27	.0196
Pre-European	32	.0203

We hope this illustrates the problems of using normalised PC scores for calculating CVs in morphological analyses. Because PC scores are inherently dimensionless, normalising them to a fixed range introduces biases that can artificially inflate or deflate CV values depending on the original sign (positive or negative) of the scores. As shown with data from Wang and Marwick (2020), by simply inverting the PC axes, which does not alter the interpretation of morphology, we see substantial changes in the calculated CV values. We propose using D_{Group} as a more appropriate approach.

References

Bonhomme, V. *et al.* 2014. Momocs: outline analysis using R. *Journal of Statistical Software* 56: 1–24. https://doi.org/10.18637/jss.v056.i13

Caloi, I. & F. Bernardini. 2024. Revealing primary forming techniques in wheel-made ceramics with X-ray microCT. *Journal of Archaeological Science* 169. https://doi.org/10.1016/j.jas.2024.106025

Cortell-Nicolau, A. *et al.* 2023. The geometric microliths of Cueva de la Cocina and their significance in the Mesolithic of Eastern Iberia: a morphometric study. *Quaternary International* 677–678: 51–64. https://doi.org/10.1016/j.quaint.2023.05.014

IGAC (Instituto Geográfico Agustín Codazzi). 2022. Base de datos vectorial básica. Colombia. Escala 1:100.000. Available at: https://www.colombiaenmapas.gov.co (accessed 8 June 2023).

Ioviţă, R. 2009. Ontogenetic scaling and lithic systematics: method and application. *Journal of Archaeological Science* 36: 1447–57. https://doi.org/10.1016/j.jas.2009.02.008

Kuhl, F.P. & C.R. Giardina. 1982. Elliptic fourier features of a closed contour. *Computer Graphics and Image* 18: 236–58.

Loftus, J.F. 2022. Reexamining ceramic standardization during agricultural transition: a geometric morphometric investigation of Initial - Early Yayoi earthenware, Japan. *Open Archaeology* 8: 1249–68. https://doi.org/10.1515/opar-2022-0273

Maya Cabrera, M.C. 2024. Proyecto: Visita ICANH, rescate hallazgo fortuito en el centro de investigaciones AGROSAVIA sitio arqueológico CIAO21, corregimiento de Obonuco-Nariño. San Juan de Pasto.

Mendoza Acosta, R. & K.H. Marín. 2023. Chronology and prehispanic Capulí funerary contexts in El Porvenir, municipality of Iles, department of Nariño, Colombia. *Jangwa Pana* 22(1): 118–38. https://doi.org/10.21676/16574923.5016

Mendoza Acosta, R. & J.C. Rubin de Rubin. 2021. Formación geoarqueológica del sitio arqueológico El Porvenir, vereda El Porvenir, municipio de Iles, departamento de Nariño (Colombia). *Arqueología y Patrimonio* 2: 53–80. https://doi.org/10.22380/26652773.2620

Oksanen, J. *et al*. 2024. vegan: community ecology package. R package version 2.6-6.1. Available at: https://CRAN.R-project.org/package=vegan

QGIS Development Team. 2022. QGIS Geographic Information System [software]. QGIS Association. Available at: http://www.qgis.org

Smallwood, A.M. *et al.* 2022. Using 3D models to understand the changing role of fluting in Paleoindian point technology from Clovis to Dalton. *American Antiquity* 87: 544–66. https://doi.org/10.1017/aaq.2022.19

Thér, R. & J. Wilczek. 2022. Identifying the contribution of rotational movement in pottery forming based on statistical surface analysis. *Archaeological and Anthropological Sciences* 14. https://doi.org/10.1007/s12520-022-01561-y

Wang, L.Y. & B. Marwick. 2020. Standardization of ceramic shape: a case study of Iron Age pottery from northeastern Taiwan. *Journal of Archaeological Science: Reports* 33. https://doi.org/10.1016/j.jasrep.2020.102554